Optimization of a piezoelectric wind-excited cantilever for energy harvesting from facades

Domenico Tommasino[1], Federico Moro[1], Enrique de Pablo Corona[2], Laura Vandi[3], Alessia Baietta[3], Alessandro Pracucci[3] and Alberto Doria[1]

[1] University of Padova, Italy
domenico.tommasino@phd.unipd.it, federico.moro@unipd.it, alberto.doria@unipd.it
[2] Smart Material GmbH, Germany
e.depablo@smart-material.com
[3] Focchi Spa, Italy
l.vandi@focchi.it, a.baietta@focchi.it, a.pracucci@focchi.it

Abstract. The optimization of the performance of a piezoelectric cantilever for energy harvesting from façades is concerned. The harvester is designed to exploit the vortex-induced vibrations due to the fluid-structure interaction between a cylindrical bluff body and the wind flow acting on the façade. An analytical lumped parameter model of the piezo-cantilever equipped with a cylindrical bluff body is provided to estimate the frequency response function between the aerodynamic tip force and the generated open circuit voltage. The analytical frequency response function is validated using experimental tests performed on a prototype of the piezo-cantilever. Finally, the design parameters of the harvester that maximize the generated voltage are determined using an optimization algorithm.

Keywords: energy harvesting, piezoelectric harvester, vortex shedding, optimization algorithm, building façade.

1 Introduction

Building industry in the last years has shown an increasing interest in smart components and in particular in smart IoT facades [1]. A smart IoT façade module is equipped with sensors that transmit data to the building management system and with actuators that modify the façade properties driving shading elements or openable vents. The final target being the improvement of the comfort of the occupants and the maximization of energetic efficiency [2, 3]. The integration of a large number of sensors and actuators on a façade requires long and complex wirings. Nowadays, an alternative to wirings is offered by energy harvesting systems that exploit the energy fluxes that usually hit a façade: thermal energy, wind energy, vibration energy. The interest in harvesters is increasing, since new environment-friendly harvesters, which do not make use of toxic elements (Pb, Bi, Te, Sb), are under development [4].
This paper deals with the development of piezoelectric harvesters able to scavenge the wind energy that hits the facade. Wind energy can be converted into electrical energy

exploiting different phenomena. In [5, 6] studies were carried out to exploit the vortex shedding phenomenon from a bluff body mounted on cantilever harvester. In [7] turbulence was exploited mimicking the behavior of grass. In [8] the fluttering of an inverted-flag piezoelectric harvester was analyzed. This paper focuses on the first phenomenon (vortex shedding) and presents the model of a cantilever harvester with cylindrical bluff body hit by a mild wind (velocity 1.4 m/s), which is typical of buildings in normal conditions. After experimental validation, the mathematical model is used for optimizing the dimensions of the harvester and a large increase in the generated voltage is obtained.

2 Mathematical model

2.1 Vortex-induced vibrations

A vortex-induced vibration is a typical fluid-structure interaction phenomenon, which affects bluff bodies in a steady fluid flow [9, 10]. For Reynolds numbers larger than 40, the formation of these vortices generates a variation in pressure around the body which results in a periodic lift force when the vortices are alternatively shed [9]. The generated aerodynamic force is orthogonal to the flow direction and can be quantified as a harmonic force on the bluff body as follows:

$$F_a(t) = \frac{1}{2}\rho_a A_c U^2 C_L(t) = \frac{1}{2}\rho_a A_c U^2 C_{L0} \sin(2\pi f_{vs} t) \tag{1}$$

where C_L is the time-dependent lift coefficient, ρ_a the fluid density, A_c the windward cross-section of the bluff body, U the fluid velocity. The parameter f_{vs} is the vortex shedding frequency and is given by the following equation:

$$f_{vs} = \frac{U S_t}{D} \tag{2}$$

in which D is a geometric parameter of the bluff body, S_t the Strouhal number [9]. The shedding of vortices synchronizes with the free movement of the structure when the f_{vs} is close to the natural frequency f_n of the structure. Large-amplitude self-sustained vibrations occur in this condition, due to the resonance phenomenon. Vortex-induced vibrations can be exploited in energy harvesting applications. f_{vs} has to match f_n of the harvester to maximize the performance of the generator. It is worth noticing that both frequencies (f_{vs}, f_n) depend on the geometry of the harvester, hence its dimensions have to be properly determined to guarantee the correct tuning.

2.2 Piezoelectric cantilever harvester with cylindrical bluff body

The harvester consists of a composite cantilever beam, made by a structural substrate covered by a piezoelectric layer, the bluff body fixed on the cantilever tip is a hollow cylinder, as shown in Figure 1. The vibration of the harvester is analyzed using a single-mode approach and only the fundamental mode is considered, since it is enough to investigate maximum performance [11]. As long as the first mode of vibration is

concerned, the displacement (y) and the rotation (φ) at the end of the beam (point P in Fig. 1) are dependent variables. The relation between y and φ is expressed by the following equation [12]:

$$y = \frac{2}{3} L_b \varphi \tag{3}$$

where L_b is the length of the cantilever beam. The composite cantilever is modeled as a mass-less spring and its corresponding moving mass, calculated using Rayleigh's method, is added to the mass of the bluff body. In these hypotheses, the harvester is simulated as a one-Degree of Freedom (DoF) mass-spring-damper system equipped with a lumped piezoelectric element, which considers the piezoelectric coupling effect [13]. The aerodynamic force F_a is schematized as a harmonic force acting on the center of the cylinder.

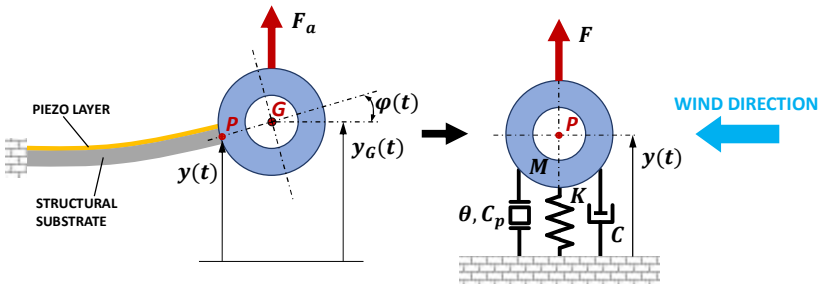

Fig. 1. Scheme of the one-DoF lumped parameter model.

The equation of motion of the lumped parameter model (4) is derived using the Lagrangian method, which allows to determine in (5) the lumped mass (M), stiffness (K), damping coefficient (C) and the Lagrangian component of the force (F) along y-direction:

$$M\ddot{y} + C\dot{y} + Ky = F \tag{4}$$

$$\begin{cases} M = \frac{33}{140}\left(\rho_b L_b w_b t_b + m_p\right) + \rho_c \frac{\pi\left(D_e^2 - D_i^2\right)}{4} L_c \left(1 + \frac{3D_e}{4L_b}\right)^2 + \frac{1}{32}\rho_c \pi (D_e^4 - D_i^4) L_c \left(\frac{3}{2L_b}\right)^2 \\ K = \frac{3EI}{L_b^3} + \frac{\theta^2}{C_p} \\ C = 2\zeta\sqrt{KM} = \frac{2\zeta K}{\omega_n} \\ F = F_a \cdot \left(1 + \frac{3D_e}{4L_b}\right) \end{cases} \tag{5}$$

where ρ_b, w_b, t_b are the density, width and thickness of the substrate, respectively; m_p the mass of the piezoelectric layer; ρ_c, D_e, D_i, L_c are the density, outer diameter, inner diameter and length of the tip hollow cylinder, respectively; E and I are the Young's modulus and the moment of inertia of the cross-section of the composite beam; ζ and ω_n are the damping ratio and the natural angular frequency of the piezo-cantilever harvester; θ is the electro-mechanical coupling coefficient [11, 12], which represents the

amount of charge per unit displacement (y) collected in the piezo-layer in open-circuit condition; C_p is the capacitance of the piezoelectric layer.

The Frequency Response Function (FRF) between the aerodynamic force F_a and the tip displacement y is calculated assuming a harmonic input:

$$FRF_y(\omega) = \frac{y_0}{F_{a,0}} = \frac{\left(1+\frac{3D_e}{4L_b}\right)}{-M\omega^2+iC\omega} = \frac{1}{K}\cdot\frac{\left(1+\frac{3D_e}{4L_b}\right)}{\left(1-\frac{\omega^2}{\omega_n^2}+2i\zeta\frac{\omega}{\omega_n}\right)} \tag{6}$$

The Open Circuit Voltage (OCV) $v_{oc}(t)$ across the terminals of the electrodes of the piezoelectric layer is expressed as follows [11]:

$$v_{oc}(t) = \frac{\theta}{C_p}\cdot y(t) \tag{7}$$

Finally, by letting (6) in (7), the FRF between the aerodynamic force F_a and the generated OCV is obtained as:

$$FRF_{v_{oc}}(\omega) = \frac{V_{oc}}{F_{a,0}} = \frac{\theta}{KC_p}\cdot\frac{\left(1+\frac{3D_e}{4L_b}\right)}{\left(1-\frac{\omega^2}{\omega_n^2}+2i\zeta\frac{\omega}{\omega_n}\right)} \tag{8}$$

The FRF between the aerodynamic force F_a and the maximum stress at clamp is given by [12, 14, 15]:

$$FRF_\sigma(\omega) = \frac{\sigma_0}{F_{a,0}} = \frac{3E}{L_b^2}h_c\cdot FRF_y(\omega) \tag{9}$$

in which h_c is the maximum distance from the neutral axis of the composite cross-section of the harvester.

3 Experimental validation

Experimental tests aimed at validating the analytical lumped parameter model. A prototype of a cantilever harvester, built by Smart Material GmbH and Focchi Spa, was used. The piezoelectric layer in the prototype consists in a Macro Fiber Composite (MFC) piezo-patch (M–8514–P2, manufactured by Smart Material GmbH) bonded to a structural substrate made by FR-4 (glass-reinforced epoxy laminate material). The bluff body is a hollow cylinder made of a polymeric material using an additive manufacturing technique. Figure 2 shows the main dimensions of the piezo-cantilever harvester used during tests. The dimensions of the piezo-patch and its electromechanical properties are available in [16].

The prototype was designed to resonate at a wind flow velocity $U = 1.4\,m/s$.

The FRF between the aerodynamic force (excitation) and the OCV (response) was measured after applying to the cylindrical tip mass in Fig. 3 an impulsive force along the vertical direction. The excitation was applied using a mini instrumented hammer for modal analysis (PCB 084A17). The two signals (applied force and OCV) were acquired using a DAQ module NI 9230 and the software NI Signal Express.

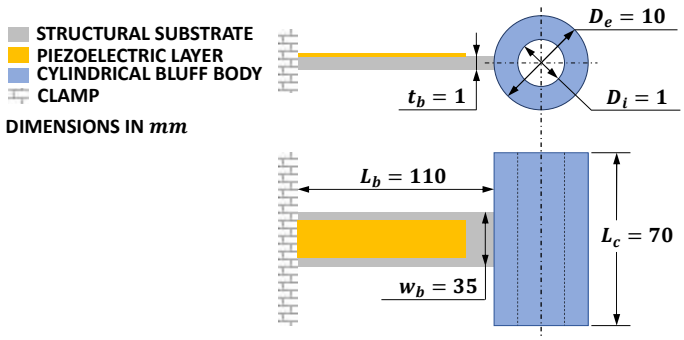

Fig. 2. Scheme of the prototype of the piezo-cantilever harvester used in experimental tests.

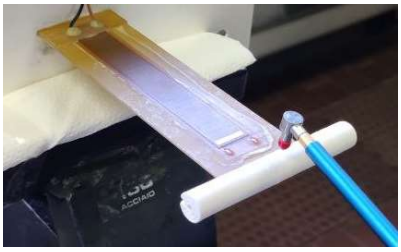

Fig. 3. An experimental test for FRF measurements.

Figure 4 shows that the analytical and experimental FRFs are in a very good agreement. It is worth highlighting that the analytical FRF is computed from (8), whereas experimental FRF is the average of the results of three tests, to limit the effect of noise and disturbances.

In table 1 the values of the natural frequency and the peak amplitude obtained in the numerical and experimental FRFs are compared. The experimental damping ratio is 0.81 % and is determined using the logarithmic decrement method.

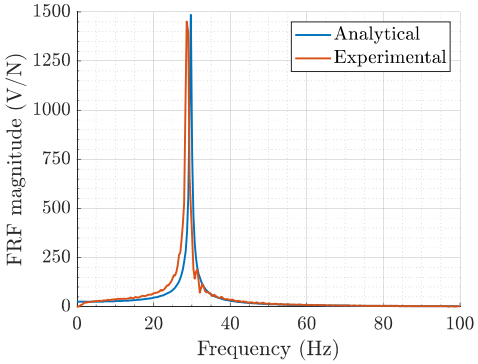

Fig. 4. Comparison between analytical and experimental FRFs. The analytical FRF is derived from (8).

Table 1. Comparison between analytical and experimental FRFs.

	Analytical	*Experimental*
Natural frequency (Hz)	29.7	28.7
FRF peak value (V/N)	1485.9	1451.6

There is a small difference between the analytical and experimental natural frequencies, because the actual constraint is not an ideal clamp and because there are small approximations in the parameters of the model.

4 Optimization algorithm

From (1) it can be noted that the aerodynamic force is proportional to the windward cross-section of the cylinder (A_c). Moreover, (7) highlights that a large displacement (y) of the end of the beam leads to a large voltage output, therefore a decrease in the natural frequency f_n (or stiffness K, see (6)) of the cantilever increases the performance of the harvester. An optimization algorithm can be defined to find the optimal dimensions of the harvester, not only to guarantee the matching between natural and vortex shedding frequencies, but also to maximize performance.
The optimization algorithm used in the framework of this research is based on the *fmincon* function available in MATLAB [17], which finds a constrained minimum of a function $FUN(X)$ of several design variables (X). It is assumed that the objective of the optimization is to maximize the generated OCV. The design variables are the dimensions of the structural substrate and hollow cylinder depicted in Fig. 2, hence $X = [w_b, t_b, L_b, D_e, D_i, L_c]$. It is worth noticing that the piezo-patch and the materials of the substrate and the cylinder are the same of the prototype. Therefore, the function $FUN(X)$ to be minimized is derived from (8) as follows:

$$FUN(X) = \frac{1}{V_{oc}(X)} = \frac{K(X)C_p}{\theta} \cdot \frac{\sqrt{\left(1-4\pi^2 f_{vs}^2 \frac{M(X)}{K(X)}\right)^2 + \left(4\pi\zeta f_{vs}\sqrt{\frac{M(X)}{K(X)}}\right)^2}}{\left(1+\frac{3D_e}{4L_b}\right)} \cdot \frac{2}{C_{Lo}\rho_a D_e L_c U^2} \tag{10}$$

The problem is subjected to linear and non-linear constraints:

$$\min\left(\frac{1}{V_{oc}(X)}\right) \quad \text{such that} \quad \begin{cases} A \cdot X \leq B \\ A_e \cdot X = B_e \\ G(X) \leq 0 \\ G_e(X) = 0 \end{cases} \tag{11}$$

in which A, A_e are matrices of coefficient and B, B_e are vectors of known constants; $G(X), G_e(X)$ are non-linear functions. The *fmincon* function starts the research of the optimum values of the parameters from the first guess values X_0 of the design variables. The solution X of the problem is found within the range defined by the lower (LB) and upper (UB) limits, that is:

$$LB \leq X \leq UB \tag{12}$$

The default algorithm interior-point is used to minimize the function FUN and no further options were specified in the *fmincon* function.

Only one linear constraint is defined, which imposes a minimum thickness of the hollow cylinder, i.e. $D_e - D_i \geq 4\ mm$. Therefore, it is imposed $A = [0\ 0\ 0 - 1\ 1\ 0]$ and $B = -4 \cdot 10^{-3}$. Three non-linear constraints are introduced:

1. The natural frequency f_n of the cantilever harvester must be tuned to the vortex shedding frequency at the given wind velocity. It is imposed that they match within a small range of frequencies, i.e.:

$$|f_n - f_{vs}| - 0.1 \leq 0 \tag{13}$$

2. The static displacement $\left(w_s = 9.81 \cdot \frac{M}{K}\right)$ at the end of the cantilever [12] must be lower than a given maximum limit:

$$w_s - 0.005 \leq 0 \tag{14}$$

3. The maximum stress at clamp σ_0 calculated using (9) must be lower than a given maximum limit:

$$\sigma_0 - 20 \cdot 10^6 \leq 0 \tag{15}$$

Table 2 shows the values used for the optimization of the parameters $X_0,\ LB,\ UB$. Table 3 shows the results of the optimization, i.e. the optimal values of the variables. The reference wind velocity is $U = 1.4\ m/s$.

Table 2. Assumed values for $X_0,\ LB,\ UB$.

	$w_b(mm)$	$t_b\ (mm)$	$L_b\ (mm)$	$D_e\ (mm)$	$D_i\ (mm)$	$L_c\ (mm)$
LB	18	0.5	100	10	0	70
X_0	35	1	110	10	1	70
UB	40	2	150	45	41	100

Table 3. Optimal values of the design variables.

w_b (mm)	t_b (mm)	L_b (mm)	D_e (mm)	D_i (mm)	L_c (mm)	f_n (Hz)	f_{vs} (Hz)	w_s (mm)	σ_0 (MPa)
18.2	1	114.9	19.9	14.5	99.9	14.8	14.8	1.1	1.0

The optimal OCV amplitude, calculated using (10) and referred to the optimal values of the design variables in Table 3, results $V_{oc,opt} = 1.83\ V$ (assuming $\rho_a = 1.225\ \frac{kg}{m^3}$, $C_{L0} = 0.3$ [10]). The OCV amplitude calculated using (10) and referred to the dimensions of the prototype (see Fig. 2) results $V_{oc} = 0.37\ V$, which is 4.9 times smaller than the optimal value. Finally, it is worth highlighting that the optimal natural frequency is smaller than the one of the prototype, whereas A_c increases, due to the larger values of both D_e and L_c. The power generated by this harvester can be estimated assuming the adoption of a SSHI converter [15]. The estimated optimal power is $P_{opt} = 4.18\ \mu W$.

5 Conclusions

The experimental tests showed that the lumped element model is able to retain the most important features of the harvester's dynamics and is suited to optimization purposes. Numerical calculations showed that optimization can lead to a large improvement in performance. The discussed methods are suited to model and optimize more complex wind harvesters composed of multiple beams and cylinders. The simulations were carried out considering constant wind velocity and the best wind direction (parallel to the harvester). The actual implementation of these harvesters on a façade requires a preliminary sensitivity analysis to assess the effect of stochastic variations of wind on the generated voltage, power and stress. Finally, the installation of an array of harvesters increases the generated power, but it has to cope with aesthetic architectural constraints.

Acknowledgments This research was funded by the H2020 InComEss project.

6 References

1. Guardigli, L. *et al.*: Sviluppo di un prototipo di facciata continua con comportamento dinamico (SmartSkin). Journal of Technology for Architecture & Environment, *16* (2018)
2. Arnesano, M., *et al.*: A sub-zonal PMV-based HVAC and façade control system for curtain wall buildings. In MDPI Proceedings (Vol. 2, No. 15, p. 1596) (2018)
3. Arnesano, M., *et al.*: Sensors and control solutions for Smart-IoT façade modules. In *20*19 IEEE International Symposium on Measurements & Networking (pp. 1-6), IEEE, (2019)
4. INCOMESS Project, INnovative Polymer-Based Composite Systems for High-Efficient Energy Scavenging and Storage. https://www.incomess-project.com/ (accessed on 21/03/2022)
5. Hobbs, W. B. *et al.*: Tree-inspired piezoelectric energy harvesting. J. Fluids Struct. 28: 103-114 (2012)
6. Akaydin, H. D. *et al.*: The performance of a self-excited fluidic energy harvester. Smart Mat. and Struct., 21(2), 025007, (2012)
7. Hobeck, J. D. *et al.*: Artificial piezoelectric grass for energy harvesting from turbulence-induced vibration. Smart Mat. and Struct., *21*(10), 105024 (2012)
8. S. Orrego, K. Shoele et al..: Harvesting ambient wind energy with an inverted piezoelectric flag. Applied Energy, 194, 212–222, (2017)
9. Blevins, R. D.: Flow-induced vibration. New York: Van Nostrand Reinhold Co (1977)
10. Païdoussis, M. P. *et al.*: Fluid-structure interactions: cross-flow-induced instabilities. Cambridge University Press (2010)
11. Erturk, A. *et al.*: Piezoelectric energy harvesting. John Wiley & Sons (2011)
12. Doria, A. *et al.*: Tuning of Vibration Energy Harvesters by Means of Liquid Masses. In: 2021 Sixteenth International Conference on EVER, IEEE pp. 1-7 (2021)
13. Akaydin, H. D. *et al.*: Energy harvesting from highly unsteady fluid flows using piezoelectric materials. J. of Intelligent Material Sys. and Struct., 21(13), 1263-1278 (2010)
14. Doria, A. et al..: Energy harvesting from bicycle vibrations by means of tuned piezoelectric generators. Electronics 9(9): 1377 (2020)
15. Tommasino, D. *et al.*: Vibration Energy Harvesting by Means of Piezoelectric Patches: Application to Aircrafts. Sensors, *22*(1), 363, (2022)
16. https://www.smart-material.com/MFC-product-propertiesV2.html (checked on 11/03/2022)
17. Bottin, M. *et al.*: Analysis and control of vibrations of a Cartesian cutting machine using an equivalent robotic model. Machines *9*(8), 162 (2021)